Int. J. Electrochem. Sci., 16 **(2021)** Article ID: 210262, doi: 10.20964/2021.01.05

International Journal of
ELECTROCHEMICAL
SCIENCE
www.electrochemsci.org

A Miniaturized Electrochemical Biosensor Based on Poly(*L*-threonine) Modified Pencil Graphite Electrodes and Its Application for Trace-Level Determination of Uric Acid, Xanthine and Hypoxanthine

Zhengcai Guo, Guiyan Wang, Jinlian Li, Dongmei Wu and Xiaoling Guo**

College of Pharmacy, Jiamusi University, Jiamusi, 154000, China.
*E-mail: guoxiaoling2004@126.com (X. Guo), dmwu@jmsu.edu.cn (D. Wu)

Received: 21 November 2019 / *Accepted:* 14 September 2020 / *Published:* 31 December 2020

A miniaturized and simple analysis tool is of vital importance for practical applications in bioanalysis. This paper describes a new strategy for the trace determination of uric acid (UA), xanthine (XA) and hypoxanthine (HX) by using miniaturized electrochemical biosensor containing a disposable pencil graphite work electrode modified with poly(*L*-threonine). The novel electrochemical device set the electrochemical detection in a 96 well plates with the microliter level of sample. Cyclic voltammetry and scanning electron microscopes were employed to characterize the biosensor. Some experimental variables of the electrode measurement parameters were optimized. Electrochemical behaviors of UA, XA and HX on the miniaturized biosensor were studied by cyclic voltammetry. The results show that the biosensor exhibited excellent electrocatalytic activity towards the oxidation of three analytes with good reproducibility, stability and wide linear region. Meanwhile, their oxidation currents linearly increase with increasing the mixture concentration from 0.500 to 100 μM for HX and 0.100 to 90.0 μM for both UA and XA with the lowest detection limit 0.50, 0.10 and 0.100 μM, respectively (S/N = 3). The miniaturized electrochemical biosensor featured easily available, low-cost material and simple fabrication, which could be applied in the trace determination of practical sample.

Keywords: Miniaturized electrochemical biosensor, Pencil graphite electrodes, Uric acid, Xanthine, Hypoxanthine

1. INTRODUCTION

As degradation product of purine metabolism in human body, xanthine (XA), hypoxanthine (HX) and uric acid (UA) have a critical function in many cellular processes [1]. The three products can penetrate cell membranes and accumulate in extracellular fluids [2, 3]. Thus, abnormal metabolic levels in body fluids such as human blood and urine can reveal some information about physiological processes

and further be used as sensitive indicators of many pathologic states. Hence, timely and accurate monitoring the change of UA, XA and HX content in body fluids may prevent and control corresponding diseases. Hence, the development of simple, sensitive and inexpensive biosensors for simultaneous determination of UA, XA, and HX is very important in the clinical point of view [4]. Conventional analytical methods available for the determination of UA, XA, and HX include enzymatic methods [5, 6], high performance liquid chromatography (HPLC) [7-9], capillary electrophoresis (CE) [10, 11] and electro-chemical analysis [12-15]. Among various methods, electroanalytical method is extremely attractive for obtaining accurate information in a simpler, efficient and cheaper manner. Because of remarkable sensitivity, compatibility, high selectivity, and label-free, electroanalytical method is ideal for the analysis of purines individually or simultaneously.

However, in the fabrication of electroanalytical biosensors, the various modified glassy carbon electrodes were used widely, poly (pyrocatechol violet)/functionalized multi-walled carbon nanotubes composite film modified electrode [16], the surface enhancement effect of mesoporous silica [17] and periodized nontronite-coated electrode [18], although most of them have shown good selectivity and sensitivities in the simultaneous determination of UA, XA and HX, the use of these working electrodes is limited by time-consuming and complex surface regeneration of electrodes, a clean and refreshed surface is very crucial for accurate and reliable analysis. Moreover, their electrochemical detection needs a relatively high sample volume owing to the limitations of using a conventional size electrode, which is a considerable drawback. The high-volume requirement not only increases the cost of testing, but also the difficulty of achieving high throughput screening. Therefore, a sensitive miniaturized electrode with the single-use and low consumption is of vital importance.

Fortunately, easy available and disposable graphite pencil electrodes (PGEs) could overcome the above problems in that the surface is easily renewed to eliminate the surface passivation by a simple mechanical replacement, and they can be carried out in very small volumes of reagents owing to inherent miniaturization, which avoids the use of additional and expensive compounds. Moreover, compared with the traditional glass carbon electrode, PGE has the advantages of wide potential window, low cost, and ease of modification [19-21]. However, PGEs are not very electrocatalytic activity toward redox reaction of some electricity molecules, the surfaces must, therefore, be modified with special electrocatalysts for enhancement of sensitivity.

Amino acid, as an electroactive species, its catalytic activity was early studied due to their special and complex structure [22]. In recent years, electrodes modified with various amino acids have been widely used for the determination of drugs, environmental pollutants, small biological molecules and so on [23-26], such as poly(methionine) for simultaneous detection of uric acid, xanthine and hypoxanthine [27], poly(*L*-aspartic acid) for dopamine and norepinephrine [28], poly(*L*-proline) for estrogen etc. [29]. As one of two proteinogenic amino acids bearing an alcohol group, electroactive polymers of threonine have also been successfully deposited onto the surface of electrode for electrocatalysis of several biology species [30-32] based on its good conductivity and low cost.

In this work, we designed a novel miniaturized electrochemical device which was adaptable to 96-well plates (Diameter, 6.94 mm) instead of traditional detection cell, and the electro-polymerized threonine film was used to improve electrochemical catalyzing properties for the oxidation of UA, XA and HX. This study is the first report of the advantages of 96-well plates and integrated three electrodes

being combined to determinate UA, XA and HX, which provides novel platform for high-through detection of smaller biomolecules from multiple perspectives.

2. EXPERIMENTAL

2.1. Reagents

UA, XA and HX were all purchased from Sigma-Aldrich (U.S.A). Threonine was sourced from Shanghai Chemical Reagent Co., Ltd. (Shanghai, China). All chemicals were of analytical grade and used without further purification. 0.200 M phosphate buffer solutions (PBS) with a series of pH were obtained by mixing stock solutions of 0.200 M KH_2PO_4 and Na_2HPO_4. All solutions were prepared with doubly distilled water. The pH measurements of solutions were conducted on a pHs-25pH-meter (Leizi Instrumental Factory, Shanghai, China).

2.2. Methods

Voltammetric measurements were performed on a CHI760B workstation (CH Instrumentation, Shanghai, China) in PBS (0. 200 M, pH = 7.00) medium by using cyclic voltammetry (CVs) and linear cyclic voltammetry (LSV) techniques. Three electrode system comprise a Pt wire as the counter electrode, an Ag/AgCl (Saturated KCl) reference electrode and ploy(*L*-threonine)/PGE (PT/PGE) working electrode, respectively. The voltammetric measurements were conducted after the PT/PGE was immersed into sample solutions for 360 s. The voltammetric response was recorded by the peak current and the average of 3.00 replicas. All experiments were accomplished at room temperature.

An S-4800 field emission scanning electron microscope (SEM, Hitachi, Japan) was used to characterize the surface morphology of the modified electrode.

2.3. Preparation of the miniaturized electrochemical biosensor

Pencil graphite (diameter of 0.500 mm, length of 60.0 mm. Chen Guang, China) wrapped with metallic wire on the end was polished with 0.050 μm alumina slurry on a wet metallographic sandpaper (size 1500 and 2000), respectively. Subsequently, it was cleaned with doubly distilled water to remove any physically adsorbed substances. An empty ballpoint pen refill was tailor made to suit as the holder, the three electrodes were integrated together with a foam plastic insulation, which can keep them on the plates firmly. Before the modification, a total of 10.0 mm of lead was immersed into the solutions and pretreated by CV in a 0.500 M H_2SO_4 solution with a potential range of −0.500 to 1.50 V at 100.0 $mV \cdot s^{-1}$ for 15.0 cycles. The polymeric film deposited on pencil graphite was obtained using CV between −0.600 and 2.30 V at 100.0 $mV \cdot s^{-1}$ for 20.0 scan cycles in pH 9.00 PBS in the present of 2.50×10^{-3} M *L*-threonine. After being washed with distilled water and air-dried, the threonine modified PGE was obtained.

3. RESULTS AND DISCUSSION

3.1. Optimization of the electro-polymerization variables

3.1.1 Effect of the electro-polymerization cycles on the biosensor response

In order to find the optimal polymerization condition of *L*-threonine, some parameters such as electro-polymerization cycles, pH of supporting electrolyte and threonine concentration were optimized by measuring the oxidation signal of XA observed with LSV technique. As shown in Fig.1A. Effect of electro-polymerization cycles was investigated by scanning the electrode within a potential range of 0.600−2.00 V in 0.200 M PBS (pH = 9.00) for 40 sequential cycles at a scan rate of 100.0 $mV \cdot s^{-1}$. The variation of LSV signal of XA versus scan cycles used in the polymerization of PGE was shown in Fig.1B. The XA oxidation signal increased with increasing the scan cycles from 10.0 to 20.0 and leveled off nearly after 20.0 scan cycles, maximum was obtained by applying 20.0 potential cycles. The reason may be associated with the increase of coverage of threonine film on the electrode surface resulting in the obstruction of electron transfer rate on the electrode surface, so the 20 potential cycles were employed for the electro-polymerization of threonine film on electrode surface.

3.1.2 Effect of the concentrations of threonine on the biosensor response

The polymerization was optimized by varying concentrations of threonine. As shown in Fig.1C, there was appreciable increase in the XA oxidation signal until concentration of *L*-threonine increased up to 250 μM. After that, almost the same XA oxidation signal was obtained at 400 μM of *L*-threonine, there was no appreciable change in the redox peak currents with increasing the concentration of *L*-threonine. Thus, 250 μM of *L*-threonine was adopted as working concentration for further studies.

3.1.3 Effect of pH on the biosensor response

The effect of solution pH on polymerization of *L*-threonine was also investigated by varying pH at 4.00, 6.00, 7.40, 9.00 and 10.5. Fig.1D showed the variation in LSV signal of XA versus pH used in the polymerization of PGE. As can been seen, the XA oxidation signal increased with increasing the pH range from 5.00−9.00, and reached its maximum at pH 9.00, then decreased as further increasing pH. Therefore, supporting electrolyte of pH 9.00 was selected in this investigation.

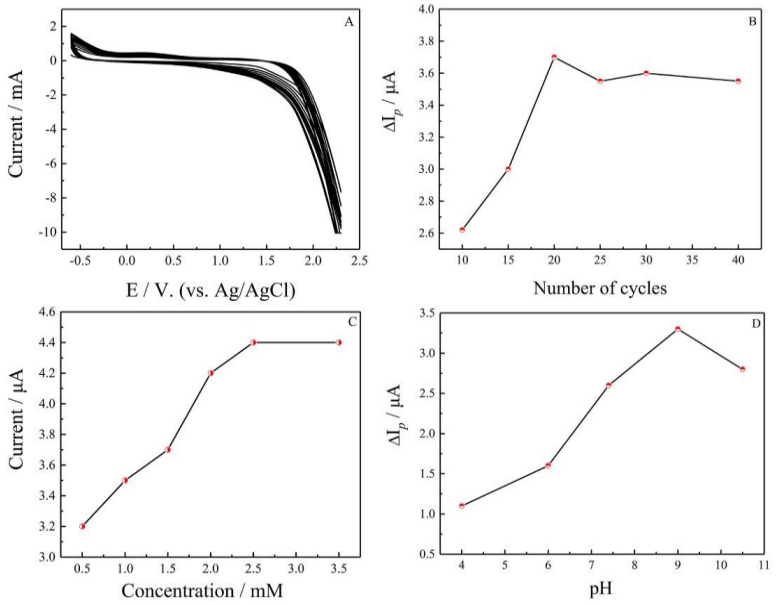

Figure 1. Electro-polymerization of threonine (40.0 cycles) on the PT/PGE (A). Effect of scanning cycles (B). Concentration of *L*-threonine (C) and pH (D) on the oxidation current of XA on the PT/PGE.

3.2. Morphologies characterization of the miniaturized biosensor

Fig.2 depicts the SEM image of modified PGE, as can be clearly seen, the modified PGE surface exhibited tiers of thin scales with small convex particles and high dense porosity. Moreover, the surface was much roughness, loose and richer in texture. This not only indicated the successful electrodeposition of *L*-threonine on the PGE surface, but also the increase of the electrode surface area. The possible formation mechanism for the electro-polymerization of *L*-threonine on PGE is proposed in Scheme 1. Thus, we can make a rational inference that the *L*-threonine is helpful to catalyze oxidation reactions of UA, XA and HX due to high number of the active sites provided by *L*-threonine for the accumulation of purine bases.

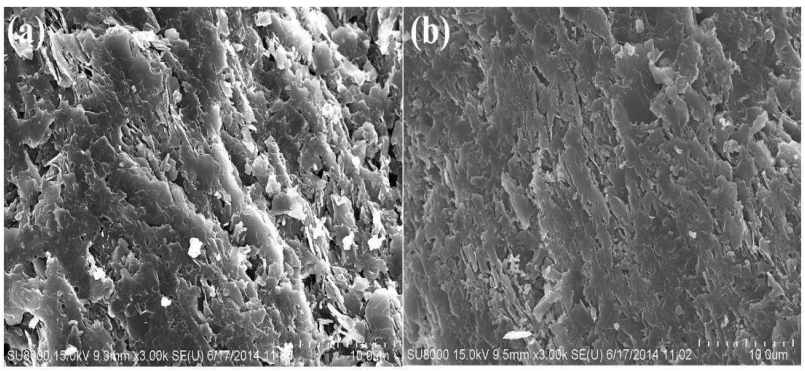

Figure 2. SEM of *L*-threonine polymerization film at PGE(a) and PT/PGE (b).

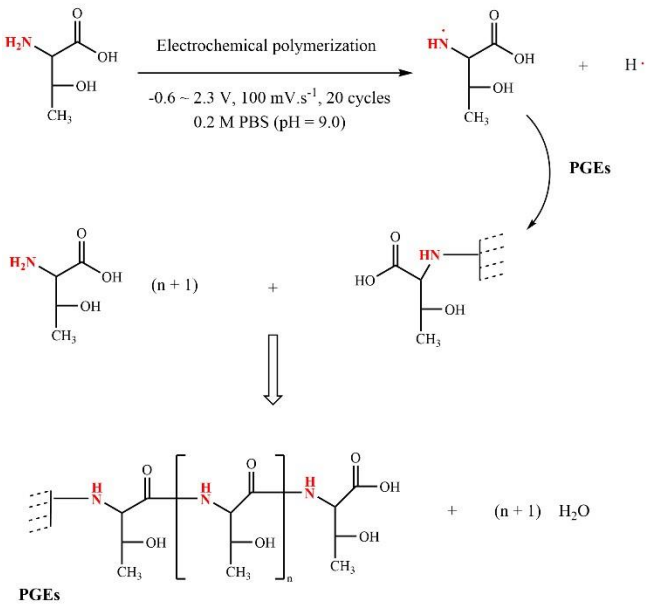

Scheme 1. Proposed polymerization structure of *L*-threonine on PGE.

3.3. Electrochemical characterization of the miniaturized biosensor

Successful preparation of PT/PGE was also confirmed by electrochemical characterization using CV. Fig.3A shows the cyclic voltammograms of PGE (a) and PT/PGE (b) obtained in the presence of 5.00 mM $[Fe(CN)_6]^{3-/4-}$ solution in 0.100 M KCl. The PGE showed a pair of poor redox peak with a peak separation (ΔE_p) of 90.0 mV, when the PGE was coated with *L*-threonine, a sharper oxidation and reduction wave was observed and the redox peak current (ΔI_p) increased significantly compared with PGE, the corresponding peak-to-peak separation value was reduced from 90 to 78.0 mV, indicating that reversibility degree of this redox system was enhanced. Furthermore, as shown in Fig.3B, background currents became larger at PT/PGE than that at PGE, implying that the *L*-threonine has been adhered to PGE surface and the surface modification with *L*-threonine plays an important role in providing the conducting bridges for the charge transfer of $[Fe(CN)_6]^{-3/-4}$, which can effectively increase the electron transfer rate of $[Fe(CN)_6]^{3-/4}$ [33, 34].

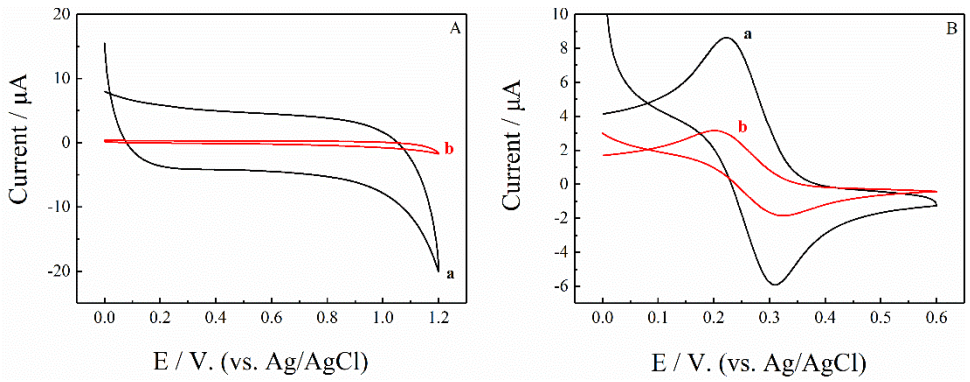

Figure 3. CVs of (A) PBS and (B) $[Fe(CN)_6]^{3-/4-}$ on PT/PGE (a) and PGE (b).

3.4. Voltammetric behavior of UA, XA and HX on the miniaturized biosensor

The electrochemical oxidation responses of coexistence of UA, XA and HX at the miniaturized biosensor in pH 6.50 PBS were investigated using LSV. As can be seen from Fig.4, peak of UA, XA and HX at the PGE was broad and small with very low peak current, whereas all of them on PT/PGE were increased significantly, suggesting formation of electropolymerized film of *L*-threonine on PGE enlarge electroactive surface area. Meanwhile, all the peak potentials of three species on PT/PGE shift slightly to more negative potential compared to PGE because poly(*L*-threonine) reduced oxidative over-potential of UA, XA and HX. So, enhanced current response showed that the poly(*L*-threonine) film indicated excellent electrocatalytic activity toward the oxidation of UA, XA and HX by accelerating the rate of electron transfer. Shift in oxidation potential towards a negative potential can be attributed to possible coordination of carboxyl group with amine groups, the poly(*L*-threonine) film has high concentration of the negatively charged surface functional carboxyl group, which could interact with the amine groups of purine derivatives by hydrogen bonding interaction. In addition, the LSV peak potential separations between UA−XA and XA−HX are 0.410 V and 0.300 V, respectively, which are large enough for the selective and simultaneous determination of UA, XA and HXA in their mixture. Hence, the as fabricated PT/PGE could be used to simultaneously determine three UA, XA and HX.

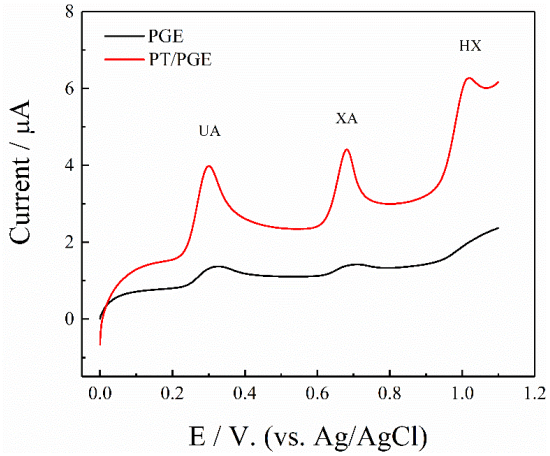

Figure 4. LSVs of PGE and PT/PGE in the presence of 25.0 μM UA, XA and 50.0 μM HX in 0.200 M PBS (pH = 6.50) at a scan rate of 50.0 $mV \cdot s^{-1}$.

3.5. Influence of scan rate on the response of UA, XA and HX at the miniaturized biosensor

CVs of UA, XA and HX on the PT/PGE with different scan rates (υ)were investigated at pH 6.50. The oxidation peak potentials shifted to a more positive potential with increasing scan rates (Fig.5A). The plots of oxidation peak currents as a function of scan rate for three molecules were displayed in the Fig.5B. In the range from 10.0 to 100 $mV.s^{-1}$, the oxidative peak current linearly increased with the scan rate, all these suggested that electrode reactions of UA, XA and HX on the PT/PGE was an adsorption-controlled electrode process. The linear regression equations relating ΔI_p with the scan rate over the range of 10.0−100 $mV.s^{-1}$ were found to be:

$$\Delta I_{p.HX}(\mu A) = 0.056 + 0.434\upsilon \quad (R^2 = 0.999) \quad (1)$$

$$\Delta I_{p.UA}(\mu A) = 0.054 - 0.313\upsilon \quad (R^2 = 0.998) \quad (2)$$

$$\Delta I_{p.XA}(\mu A) = 0.028 - 0.122\upsilon \quad (R^2 = 0.999) \quad (3)$$

In addition, it was observed that the ΔE_p all shift to more positive potentials with increase of scan rate for the three purine derivatives, suggesting a kinetic limitation in the reaction between the oxidation sites and PGE. Meanwhile, there's a good linear relationship between the catalytic oxidation peak potentials of UA, XA and HX and the corresponding natural logarithm of scan rates ($\ln \upsilon$), respectively, which confirms the irreversibility of the oxidative process [35, 36].

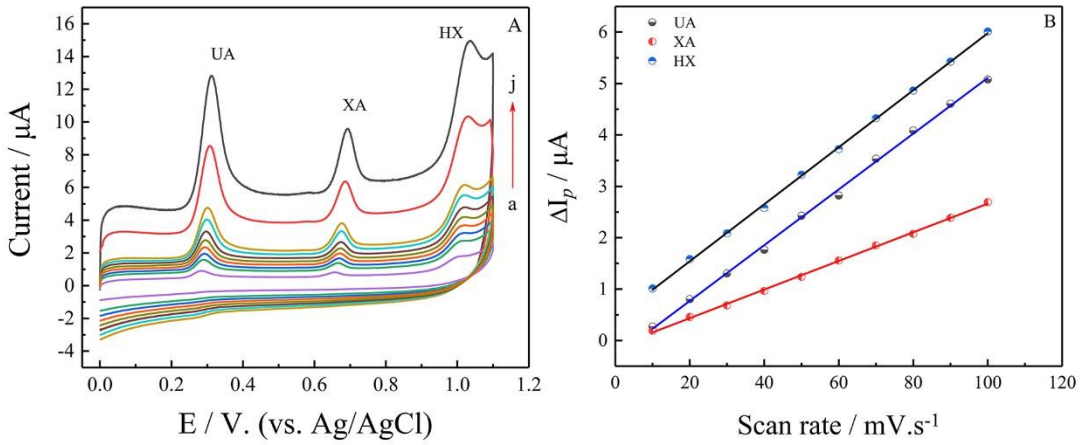

Figure 5. Influence of scan rate on the response of UA, XA and HX at the PT/PGE. (A) CVs of 50.0 μM UA, 25.0 μM XA and 50.0 μM HX at PT/PGE with a scan rate of (a–j: 10.0, 20.0, 30.0, 40.0, 50.0, 60.0, 70.0, 80.0, 90.0, 100 mV s^{-1}). (B) Plots of the oxidative peak current versus the scan rate in pH 6.50 PBS.

3.6. Influence of the solution pH on the response of UA, XA and HX at the miniaturized biosensor

Effect of solution pH on the simultaneous determination of UA, XA and HX was investigated. The effect of pH on electrocatalytic responses of UA, XA and HX on the PT/PGE in the 5.50 to 9.50 pH range was investigated by LSV. As shown in Fig.6A, both the ΔE_p and ΔI_p for 25.0 μM UA, 50.0 μM XA and HX were influenced by the solution pH. With increasing pH from 5.50 to 9.50, it was easily found that the ΔE_p of all three purine derivatives shifted negatively and decreased linearly with the increase of pH values, indicating that protons are directly involved in the rate determination step of the oxidation reaction of three species (Fig.6B). The equations relating ΔE_p with pH were:

$$\Delta E_{p.HX}(V) = 1.44 - 0.050pH \quad (R^2 = 0.994) \quad (4)$$

$$\Delta E_{p.XA}(V) = 1.10 - 0.053pH \quad (R^2 = 0.995) \quad (5)$$

$$\Delta E_{p.UA}(V) = 0.705 - 0.052pH \quad (R^2 = 0.992) \quad (6)$$

It could be seen that the slope was 52.0 mV pH^{-1} for UA, 53.0 mV pH^{-1} for XA, 50.0 mV $pH^{-1}$for HX, which were approached to the theoretical value of 59.0 mV pH^{-1}, proving that the electrode reactions of the three substances are participated by proton hydrogen with an equal number of protons. For electrochemical reaction affected by pH, the corresponding Nernst equation was expressed as

follows:

$$E_{red} = E_{red}{}^{0} + \frac{RT}{nF}\ln\frac{[Ox]}{[\mathrm{Red}]} + 2.303\frac{mRT}{nF}\mathrm{pH} \qquad (7)$$

where E_{red} is the half-cell reductive potential, E^0_{red} is the standard half-cell reductive potential, Ox and Red are the oxidized and reduced substances, respectively, n is the number of electrons transferred in the electrode reaction, m is the number of protons in the electrode reaction. The relationship between E_p and pH could be further expressed by its slope $dE_p/\mathrm{dpH} = (-2.303\,mRT)/(nF)$, and the *m/n* values was also calculated using equation mentioned-above and slope, the three values were 0.850 for UA, 0.890 for XA, and 0.870 for HX, respectively. All of them are close to 1.00, indicating that an equal number of electrons and protons attending in the electrochemical oxidation process, which was the same as previous reports [36, 37]. Meanwhile, the peak currents for UA, XA and HX increased with increasing pH value from 5.50 to 6.50 until the peak currents reached the highest peak at pH 6.50 for all the three species, then decreased with further increase in pH value (Fig.6C). In consequence, in order to achieve the higher catalytic activity of the poly(*L*-threonine) film, pH 6.50 PBS was chosen for electrocatalytic oxidation of XA, HX and UA simultaneously.

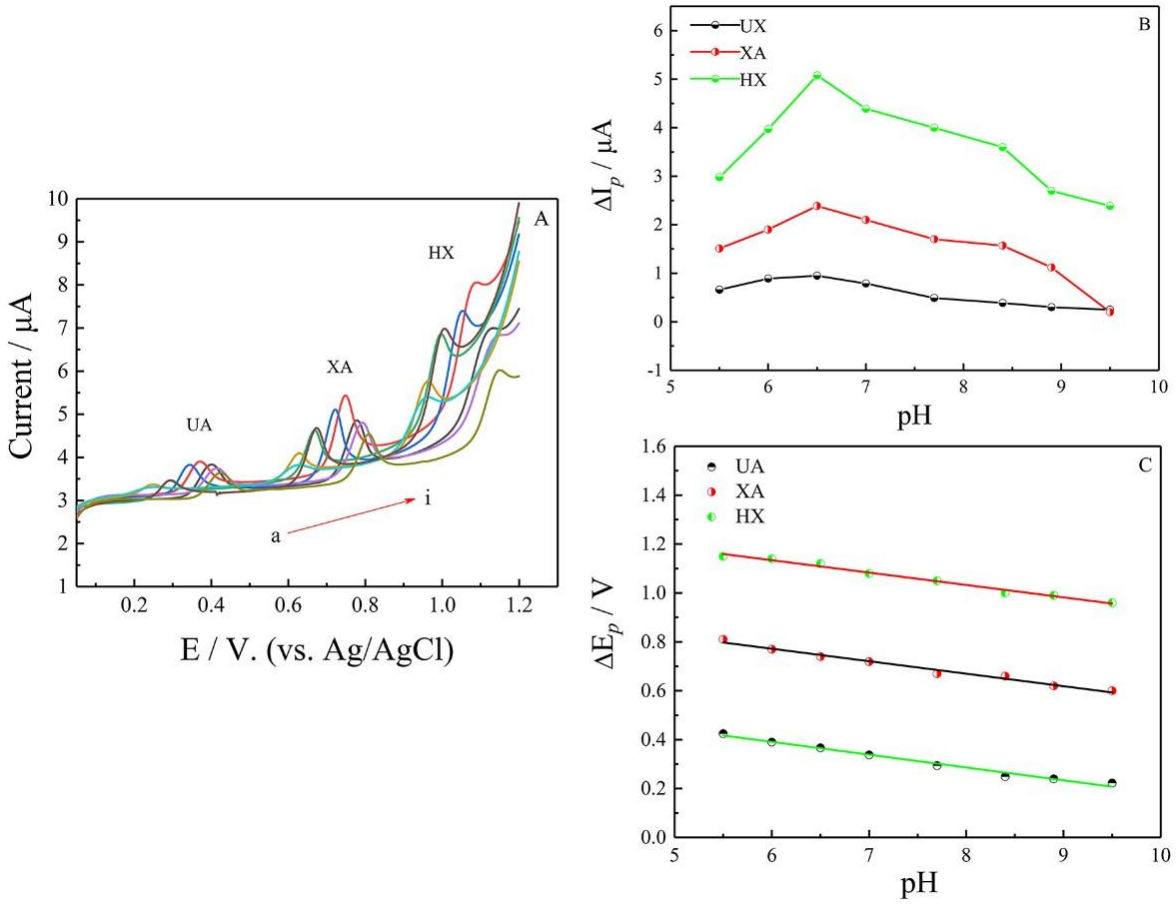

Figure 6. Influence of the solution pH on the response of UA, XA and HX at the PT/PGE. (A) Effects of pH on the LSVs. (B) Anodic peak current and anodic peak potential (C) of 25.0 μM UA, 50.0 μM XA and HX on PT/PGE, respectively. Scan rate: 50.0 mV. s^{-1}, 0.200 M PBS.

3.7. Anti-interference determinations of UA, XA and HX at the miniaturized biosensor

Under optimum conditions, a series of mixture solutions of UA, XA and HX were scanned at a scan rate of 50.0 $mV \cdot s^{-1}$ by varying the concentration of one molecule while the concentrations of the other two remaining unchanged. As shown in Fig.7A, the anodic current of UA increased with the increase in its concentration from 0.100 to 80.0 μM, while maintaining the concentration of HX and UA constant at 30.0 μM. No obvious interference was observed for the determination of UA in the presence of HX and XA. Similarly, Fig.7B (and 7C) showed that the peak current responses of XA and HX increase linearly with the increase in their contents, while the peak currents of the other two keep nearly constant, which indicated that the presence of any one compounds do not interfere with the response of the other compounds. Therefore, the PT/PGE possessed strong anti-interference in the selective determinations of UA, XA and HX.

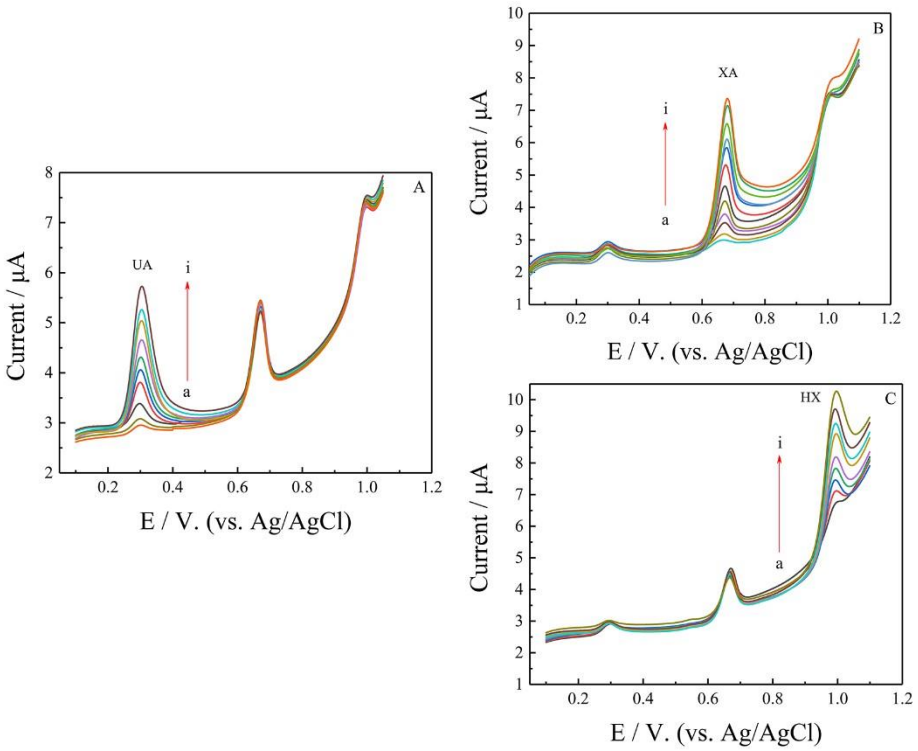

Figure 7. LSVs at PT/PGE in pH 6.50 PBS containing (A) 30 μM XA, HX and various concentrations of UA (a−i): 0.100, 0.200, 2.00, 10.0, 20.0, 30.0, 50.0, 70.0 and 80.0 μM. (B) 30 μM UA, HX and various concentrations of XA (a−i): 0.200, 2.00, 10.0, 20.0, 30.0, 50.0, 70.0, 90.0 and 100 μM. (C) 10.0 μM UA, XA and various concentrations of HX (a−i): 0.500, 5.00, 10.0, 30.0, 40.0, 50.0, 60.0, 80.0 and 100 μM.

The anti-interference ability of the PT/PGE electrode toward the detection of UA, XA and HX in the presence of a few possible interfering compounds, such as urea, glucose, oxalic acid, caffeine and some inorganic substances, such as NaCl, KNO_3, $Mg(NO_3)_2$ and so on was evaluated. The results showed that no obvious fluctuation of current response was detected for 10.0 μM of UA, XA and HX in the presence of 100 μM of interferents, indicating that the PT/PGE is highly selective toward the determination of three analytes (data not shown).

3.8. Simultaneous determination of UA, XA and HX at the miniaturized biosensor

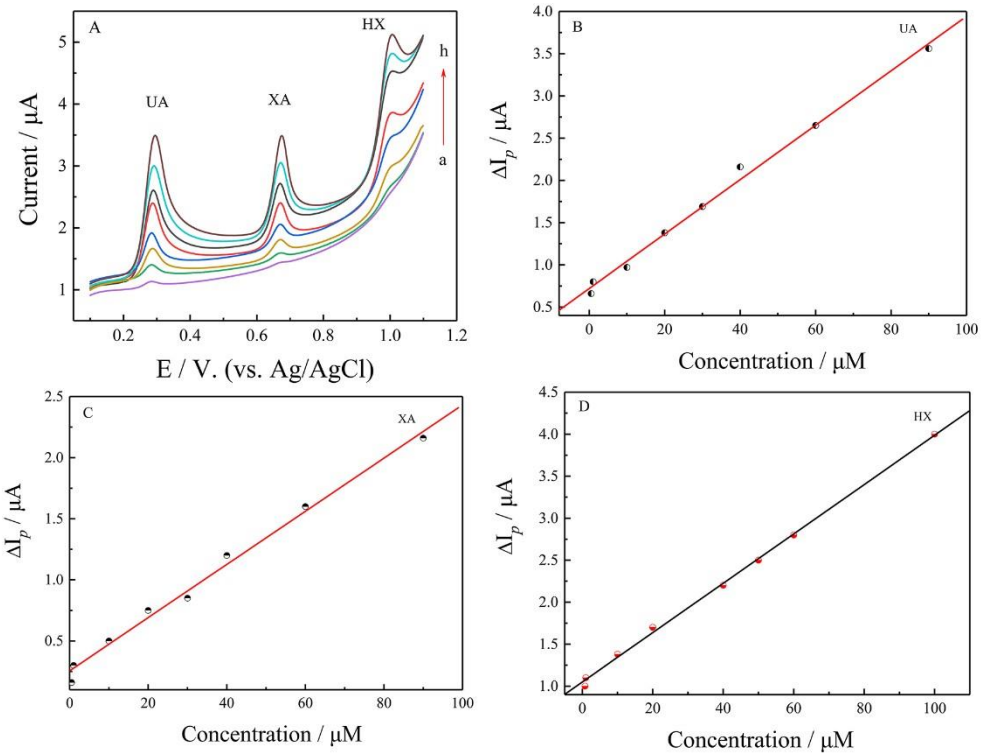

Figure 8. Simultaneous determination of UA, XA and HX at the PT/PGE. (A) LSVs obtained for the simultaneous dilution of 80.0 μM of UA, XA and 90.0 μM of HX at PT/PGE in 0.200 M of PBS solution (pH = 6.50). Concentration calibration curve of the LSV current response for (B) UA, (C) XA and (D) HX. Concentrations of UA, XA (a−h: 0.100, 1.00, 10.0, 20.0, 30.0, 40.0, 60.0, 90.0 μM) and HX (a−h: 0.500, 1.00, 10.0, 20.0, 40.0, 50.0, 60.0, 100 μM).

To investigate the linear ranges and the detection limits for simultaneous detection of UA, XA and HX on the miniaturized biosensor, LSV peak current responses of UA, XA and HX by simultaneous varying concentrations of three species in a mixture have been measured. As shown in Fig.8, the peak currents for oxidations of UA, XA and HX increased proportionally with increasing their concentrations. The linear relationships between the ΔI_p and concentrations of HX, UA and XA are respectively:

$$\Delta I_{p.XA}(\mu A) = 0.256 - 0.022 C_{XA} \quad (R^2 = 0.996) \quad (8)$$

$$\Delta I_{p.UA}(\mu A) = 0.721 - 0.032 C_{UA} \quad (R^2 = 0.997) \quad (9)$$

$$\Delta I_{p.HX}(\mu A) = 1.05 + 0.029 C_{HX} \quad (R^2 = 0.999) \quad (10)$$

The linear ranges for simultaneous detections of UA, XA and HX are 0.100−90.0 μM, 0.100−90.0 μM and 0.500−100 μM, respectively. The linear range for detection of UA, XA and HX by this miniaturized biosensor spans 3 orders of magnitude, which are similar with or much wider than some of those published sensors. The corresponding detection limits for UA, XA and HX are 0.100, 0.100, and 0.500 μM, respectively. These values are comparable to most of those found in literature for the three analytes using other electrodes (Table 1). However, most electrodes in these studies are usually

time consuming, and require expensive material and high dose of sample.

Table 1. Comparison of different chemically modified electrodes for the determination of XA, HX and UA.

Electrode	Methods	Analytes	Linear range	Detection limit	Reproducibility	Ref.
			μM	μM	RSD (%)	
		UA	0.1−800	0.199	1.8	
[a] Au-PEDOT-fMWCNT/GCE	DPV	XA	0.05−175	0.024	2.7	38
		HX	0.1−150	0.091	2.1	
		UA	0.10−25.0	0.03	1.86	
[b] EPPGE	SWV	XA	0.10−50.0	0.06	2.93	39
		HX	0.10−50.0	0.08	4.84	
		UA	2.00−80.0	0.014	1.50	
[c] DGPE	DPV	XA	1.00−40.0	0.005	1.59	40
		HX	0.100−10.0	0.005	3.10	
		UA	2.00−10.0	0.767	2.17	
[d] $CoFe_2O_4$/rGO/GCE	DPV	XA	2.00−10.0	0.650	2.04	41
		HX	2.00−10.0	0.506	2.33	
		UA	0.500−60.0	0.400	1.90	
[e] CMC-Pal-NG/GCE	DPV	XA	0.200−20.0	0.050	3.60	37
		HX	0.600−55.0	0.400	1.30	
		UA	1.00−2200	0.430	2.10	
[f] Co-CeO_2/GCE	SWV	XA	0.10−1000	0.470	1.90	42
		HX	1.00−600	0.260	2.50	
		DA	1.00−200	0.050	2.50	
		UA	2.00−1600	0.060	3.10	
[g] P6-TG/GCE	DPV	XA	1.00−500	0.300	2.30	43
		HX	2.00−800	0.100	2.80	
		UA	0.100−90.0	0.100	1.90	
Poly(*L*-threonine)/PGE	LSV	XA	0.100−90.0	0.100	3.20	**This work**
		HX	0.500−100	0.500	0.70	

Note:
[a] Functionalized multi-walled carbon nanotube (fMWCNT) stabilized nanogold (Au) decorated PEDOT: TOS polymeric nanocomposite modified glassy carbon electrode (Au-PEDOT-fMWCNT/GCE).
[b] Edge plane pyrolytic graphite electrode (EPPGE).
[c] Disposable graphite pencil electrode (DGPE).
[d] Cobalt ferrite ($Co_2Fe_2O_4$)/reduced graphene oxide (rGO) modified glassy carbon electrode ($Co_2Fe_2O_4$/rGO/GCE).
[e] Carboxymethyl cellulose (CMC) decorated both palygorskite (pal) and nitrogen doped graphene (NG) modified glassy carbon electrode (CMC-Pal-NG/GCE).
[f] Co doped CeO_2 nanoparticles modified glassy carbon electrode (Co-CeO_2/GCE).
[g] Polymerized 6-thioguanine (6-TG) modified glassy carbon electrode (P6-TG/GCE).

Therefore, although the detection limit is not low enough to detect nanomolar concentration of UA, XA and HX, a lot of improvement regarding characteristics of the developed miniaturized biosensor including its cost effectiveness, disposable use and wide material source made it a perfect candidate for simultaneous detection of UA, XA and HX when compared with other methods in Table1.

3.9. Reproducibility and batch parallelism

The repeatability of the miniaturized biosensor was examined by 30.0 consecutive measurements of XA (30.0 μM) and the result showed the percentage of approximately 15.0% degradation. The batch differences of individual electrodes were investigated by using five different electrodes prepared independently. The recorded LSVs displayed a small batch differences with an RSD of 2.70%, indicating that the miniaturized biosensor has good repeatability and batch parallelism.

4. CONCLUSIONS

For the first time, a miniaturized electrochemical biosensor was constructed by combining an integrated three-electrode and a 96-well plate for simultaneous determination of uric acid (UA), xanthine (XA) and hypoxanthine (HX), in which the usage of samples is saved from 1.00 mL in the traditional device to 100 μL. The enhanced oxidation currents and lowered oxidation over-potentials indicated poly(*L*-threonine) modified PGE exhibited high electrocatalytic activities toward the oxidations of HX, XA and UA, meanwhile, the sensor showed wide linear range, low detection limit, excellent reproducibility and stability. Moreover, the miniaturized electrochemical biosensor had such advantage of being cheap, simplicity, commercial availability and fast electrode surface 'Regeneration' that it could be for disposable applications in routine analysis. Hence, the miniaturized electrochemical biosensor could be used as a cheap alternative to commercially available traditional electrodes for analysis of valuable biological samples.

ACKNOWLEDGEMENTS
This work was supported by the Funds of NSFC from China [21777060], Key teachers project of Jiamusi University [JMSURCGG2016-002].

AUTHOR CONTRIBUTIONS
Xiaoling Guo * and Dongmei Wu ** revised the manuscript. All authors have given approval to the final version of the manuscript.

CONFLICTS OF INTEREST
There are no conflicts to declare.

References

1. G. Burnstock, *Drug Development Research*, 28(1993)195. doi:10.1002/ddr.430280303.
2. E.J. Wood, *Biochemistry and Molecular Biology Education*, 32(2004)62. doi:10.1002/bmb.2004.494032010298.
3. Y. Wang, L.-l. Tong, *Sensors and Actuators B: Chemical*, 150(2010)43. https://doi.org/10.1016/j.snb.2010.07.044
4. C. Chen, J.-M. Lü, Q. Yao, *Medical Science Monitor*, 22(2016)2501. doi:10.12659/MSM.899852.
5. R.A. Chalmers, R.W.E. Watts, *Analyst*, 93(1968)354. doi:10.1039/AN9689300354.
6. J.M. Amigo, J. Coello, S. Maspoch, *Analytical and Bioanalytical Chemistry*, 382(2005)1380. doi:10.1007/s00216-005-3275-4.

7. N. Cooper, R. Khosravan, C. Erdmann, J. Fiene, J.W. Lee, *Journal of Chromatography B*, 837(2006)1.
doi:10.1016/j.jchromb.2006.02.060.
8. Y. Wang, M. Deng, B. Deng, L. Ye, X. Fei, Z. Huang, *Journal of Clinical Laboratory Analysis*, 33(2019)1.
doi:10.1002/jcla.22868.
9. M.S. Rashed, A.A.A. Saadallah, Z. Rahbeeni, W. Eyaid, M.Z. Seidahmed, S. Al-Shahwan, M.A.M. Salih, M.E. Osman, M. Al-Amoudi, L. Al-Ahaidib, M. Jacob, *Biomedical Chromatography*, 19(2005)223.
doi:10.1002/bmc.439.
10. Y. Tao, X. Zhang, J. Wang, X. Wang, N. Yang, *Journal of Electroanalytical Chemistry*, 674(2012) 65.
https://doi.org/10.1016/j.jelechem.2012.03.009.
11. C. Bory, C. Chanting, R. Boulieu, *Journal of Chromatography A*, 730(1996)329.
doi:10.1016/0021-9673(95)01086-6.
12. G. Pierini, S. Robledo, M. Zon, M. Nezio, A. Granero, H. Fernández, *Microchemical Journal*, 138(2018)58.
doi:10.1016/j.microc.2017.12.025.
13. Y. Wen, J. Chang, L. Xu, X. Liao, L. Bai, Y. Lan, M. Li, *Journal of Electroanalytical Chemistry*, 805(2017).
doi:10.1016/j.jelechem.2017.09.053.
14. S. Hason, V. Ostatna, M. Fojta, *Electrochimica Acta*, 329(2019)135132.
doi:10.1016/j.electacta.2019.135132.
15. R. Ojani, A. Alinezhad, Z. Abedi, Sensors and Actuators B: Chemical, 188(2013)621.
https://doi.org/10.1016/j.snb.2013.07.015.
16. B. Fang, N. Zhang, W. Zhang, A. Gu, G. Wang, *Journal of Applied Polymer Science*, 112(2009)3488.
doi:10.1002/app.29929.
17. X. Dai, F. Qiu, X. Zhou, Y. Long, W. Li, Y. Tu, *Analytica Chimica Acta*, 848(2014)25.
https://doi.org/10.1016/j.aca.2014.08.002.
18. R. Thangaraj, A.S. Kumar, *Analytical Methods*, 4(2012)2162.
doi:10.1039/C2AY25029B.
19. M.R. Akanda, M. Sohail, M.A. Aziz, A.-N. Kawde, *Electroanalysis*, 28(2016)408.
doi:10.1002/elan.201500374.
20. M.d. Vestergaard, K. Kerman, E. Tamiya, *Analytica Chimica Acta*, 538(2005)273.
https://doi.org/10.1016/j.aca.2005.01.067.
21. J. Wang, A.N. Kawde, E. Sahlin, *The Analyst*, 125(2000)5.
doi:10.1039/A907364G.
22. T. Kokab, A. Shah, F. Iftikhar, J. Nisar, M. Akhter, S. Khan, *ACS Omega*, 4(2019)22057.
doi:10.1021/acsomega.9b03189.
23. J.M. Asara, G.Q. Daley, L.C. Cantley, *Science*, 339(2013)222.
doi:10.1126/science.1226603.
24. Y. Li, Z. Ye, J. Zhou, J. Liu, G. Song, K. Zhang, B. Ye, *Journal of Electroanalytical Chemistry*, 687(2012)51.
https://doi.org/10.1016/j.jelechem.2012.09.045.
25. Y. Gao, H. Li, J. Tong, L. Wang, *Environmental Technology*, (2019)1.
doi:10.1080/09593330.2019.1701569.
26. J. Soleymani, M. Hasanzadeh, M. Eskandani, M. Khoubnasabjafari, N. Shadjou, A. Jouyban, *Materials Science and Engineering: C*, 77(2017)790.
https://doi.org/10.1016/j.msec.2017.03.257.

27. A.A. Ensafi, E. Heydari-Bafrooei, M. Dinari, S. Mallakpour, J*ournal of Materials Chemistry B*, 2(2014)3022.
doi:10.1039/C3TB21827A.
28. R. Ojani, A. Alinezhad, Z. Abedi, *Sensors and Actuators B: Chemical*, 188(2013)621.
https://doi.org/10.1016/j.snb.2013.07.015.
29. Z. Yu, X. Li, X. Wang, X. Ma, X.I.A. Li, K. Cao, *Journal of Chemical Sciences*, 124(2012)537.
doi:10.1007/s12039-011-0179-z.
30. L. Luo, F. Li, L. Zhu, Y. Ding, D. Deng, *Sensors and Actuators B: Chemical*, 187(2013)78.
https://doi.org/10.1016/j.snb.2012.09.056.
31. S. Chitravathi, B.E. Kumara Swamy, G.P. Mamatha, B.N. Chandrashekar, *Journal of Molecular Liquids*, 172(2012)130.
https://doi.org/10.1016/j.molliq.2012.03.022.
32. Y. Hua, Z. Song, J. He, Y. Zhang, C. Hu, *Advanced Materials Research*, 813(2013)413.
https://doi.org/10.4028/www.scientific.net/AMR.813.413.
33. S.-G. Sun, L. Yao, Q.-H. Wu, Z.-Q. Tian, *Langmuir*, 18(2002)6274.
doi:10.1021/la025817f.
34. T. Mathavan, S. Umapathy, M.A. Jothirajan, M.F. Parveen, T.S. Vivekanandam, A. Soni, G.S. Okram, V. Ganesan, *Materials Letters*, 64(2010)2009.
https://doi.org/10.1016/j.matlet.2010.06.009.
35. D. Zhu, H. Ma, H. Pang, L. Tan, J. Jiao, T. Chen, *Electrochimica Acta*, 266(2018)54.
https://doi.org/10.1016/j.electacta.2018.01.185
36. H. Ibrahim, Y. Temerk, *Journal of Electroanalytical Chemistry*, 780(2016).
doi:10.1016/j.jelechem.2016.09.016
37. Y. Wen, J. Chang, L. Xu, X. Liao, L. Bai, Y. Lan, M. Li, *Journal of Electroanalytical Chemistry*, 805(2017).
doi: 10.1016/j.jelechem.2017.09.053.
38. S. Sen, P. Sarkar, *Analytica Chimica Acta*, 1114(2020)15.
https://doi.org/10.1016/j.aca.2020.03.060.
39. G.D. Pierini, S.N. Robledo, M.A. Zon, M.S. Di Nezio, A.M. Granero, H. Fernández, *Microchemical Journal*, 138(2017)58.
https://doi.org/10.1016/j.microc.2017.12.025.
40. N.A. Odewunmi, A.-N. Kawde, M. Ibrahim, Electroanalysis, 30(2018)2311.
doi: 10.1002/elan.201800397.
41. N.T.V. Hoan, N.N. Minh, N.T.H. Trang, L.T.T. Thuy, C. Van Hoang, T.X. Mau, H.X.A. Vu, P.T.K. Thu, N.H. Phong, D.Q. Khieu, Journal of Nanomaterials, 2020(2020)9797509.
doi: 10.1155/2020/9797509.
42. N. Lavanya, C. Sekar, R. Murugan, G. Ravi, Materials Science and Engineering: C, 65(2016) 278.
https://doi.org/10.1016/j.msec.2016.04.033.
43. D. Lan, L. Zhang, *Journal of Electroanalytical Chemistry*, 757(2015)107.
https://doi.org/10.1016/j.jelechem.2015.09.018.